Deep Learning-Based Super-Resolution of Digital Elevation Models in Data Poor Regions.

Ashok Dahal[1*], Bastian Van Den Bout[1], Cees Van Westen[1], Michael Nolde[2]

1 Faculty of Geoinformation Science and Earth Observation, University of Twente

2 German Remote Sensing Data Center, German Aerospace Center

Abstract

In order to develop reliable models, the geoscientific community requires high-resolution data sets. However, the collection of such data is a persistent challenge due to the limitations of resources. The concept of super-resolution, a method from the field of machine learning, can be used to predict a high-resolution version of a low-resolution dataset to improve usability in geoscientific applications. However, thus far, super-resolution is predominantly used in image data with few cases on improving the scientific data but focusing on improving quality of same downsampled data. More importantly, it is unknown whether models that are developed and trained with high-resolution data of specific locations can also be applied to data-poor regions. To address these gaps, this study investigated the use of deep learning-based super-resolution to improve the resolution of digital elevation data, focusing on the question whether models trained with high resolution data can also be applied to regions for which only low-resolution data are available. We focused on Digital Elevation Models (DEMs), as these are among the most important datasets for many geoscientific applications and used two of the most advanced Super-Resolution models (EBRN and ESRGAN) from different groups of deep learning architecture. We trained those models extensively using high-resolution LiDAR DEM data from Austria, and found that, for the Austrian study sites, these models performed better than commonly used interpolation techniques such as bicubic interpolation. To test model applicability to different terrain conditions, we applied the models developed and trained with Austrian data to globally available free datasets on/for Colombia and Dominica. A novel loss function, training technique and evaluation metrics were developed to train and evaluate the results focusing on improving DEM data. Our results show that super-resolution can improve the accuracy of global datasets by 30-50% relative to bicubic interpolation, thus providing a promising solution for locations for which only low-resolution DEM data are available.

Keywords: DEM Data, Super Resolution, Deep Learning,Geo-Data Processing

1 Introduction

Geoscience community mostly faces with the problem of data unavailability in sufficiently high resolution in most of the research projects in the global south. Even though global data are available, they do not have sufficient resolution to provide local details. Which could be improved by using data improvement techniques such as Super Resolution methods. Super Resolution is a data processing technique which can improve spatial and spectral domain of the data in question.

As one of the earliest works on the Super-Resolution of Digital Elevation Models (DEMs), Bulyshev et al. (2011; 2014) developed a technique to improve the spatial resolution of Flash LIDAR. NASA used the this approach for the Super-Resolution purely based on multi-frame matching and mathematical projection (Bulyshev et al., 2011). Liu et al. (2018) used Super-Resolution for the lunar surface reconstruction using the improved sparse representation. Some works on DEM Super-Resolution used Convolution Neural Network (CNN) (Moon & Choi, 2016; Xu et al., 2019) and approaches based on Generative Adversarial Networks (GAN) (Demiray et al., 2020; Leong & Horgan, 2020; Shin & Spittle, 2019a). However, the major problem with those approaches is that they apply the super-resolution techniques on DEMs obtained from the same source and at the same location (Kubade et al., 2020, 2021; Shin & Spittle, 2019b; Xu et al., 2019). The models resulting from using super resolution on a downgraded set of available high-resolution data are not applicable in the real-world, where the aim is to improve the quality of data for locations where high resolution data is not available or inaccessible. Testing the model at the same location as it is trained also does not provide full information on the applicability of such methods to improve the quality of the freely available global dataset. Some researchers also used Shuttle Radar Topography Mission (SRTM) data which is available freely for super-resolution applications (Jiao et al., 2020; Wu & Ma, 2020), but in these cases, super sampling was done at very low resolution, producing a final resolution of 30 by 30 meters, which is too low for most/ many geoscience modelling studies.

In existing literature, most researchers analyzed the output DEMs from super-resolution via ‘Peak Signal to Noise Ratio’ (PSNR) for comparing the similarity between two images. The Structural Similarity Index Measure (SSIM), which is an important metric for understanding the quality of images (Kubade et al., 2020, 2021; Shin & Spittle, 2019b; Xu et al., 2019) has been used much less, due to the very large range of elevation. While computing with just the elevation values, SSIM will saturate and provide almost perfect values for almost all kinds of DEM. Thus, there is a need for evaluation metrics that consider the raw elevation as well as the derivative products such as Slope, Aspect and Hillshade, which are often used in geoscientific modelling approaches.

This study aimed to increase the usability of globally available DEM datasets for geoscientific modelling by increasing the spatial resolution of input datasets, using deep learning-based Super-Resolution techniques. Specifically, we explored whether models trained with high-resolution data from one region can be applied to parts of the world where high-resolution data collection is challenging due to technological and financial limitations. To this end, we adapted two Super-Resolution models for downscaling global digital elevation datasets to a higher resolution. The models were trained with a High-Resolution LiDAR DEM in Austria and the trained model was used to test its applicability in improving the freely available global DEM for two different regions (Dominica and Colombia). We also tested new approaches to evaluate the quality of Super-Resolution output DEMs, comparing to the global dataset with respect to measured high-resolution datasets of the two application areas (Dominica and Colombia). Furthermore, we developed novel methodologies to train and evaluate the super-resolution methods specifically for DEM datasets using elevation and its derivatives.

2 Dataset Description

For training the deep learning network, high-resolution data were requiredfrom mountainous locations with sufficient terrain variability. For this purpose, we collected the freely available 5-meter resolution LiDAR data from Austria (for the province of Carinthia generated in 2015, for Salzburg in 2016, and for Tyrol in 2018) and selected six catchments with slopes in three classes (0-30, 30-50, and 50-70 degrees). We also selected a square region with sufficient terrain variability to test the unbiased quality of the model performance. The DEMs for these areas were resampled to lower resolution data using the Bicubic Interpolation function of MATLAB and then further converted to patches of 128x128 pixels for High Resolution (HR) samples and 32x32 for Low Resolution (LR) samples. Wang et al. (2018) have shown that using higher size patches is better for training larger networks because it can provide more information about the local geographical characteristics of the terrain, which enables the model to learn about geographic relationships. The regions selected for training the deep learning model are shown in Figure 1.

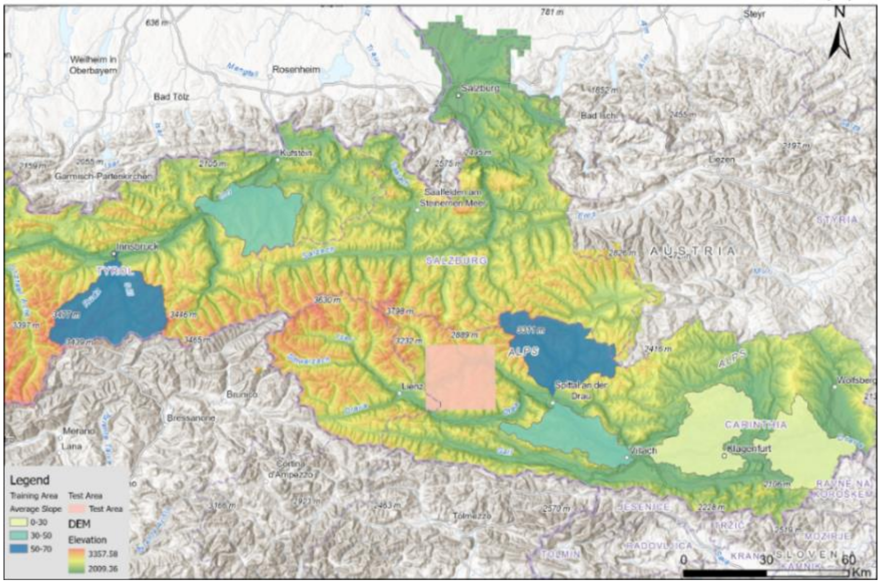

Figure 1: Training and test data samples from Austria LiDAR Data. Basemap sources: ESRI, HERE, OpenStreetMap

We also selected two sites representative for data-scarce regions, for which we also could access a high-resolution DEM for quality assessment, and which were recently impacted by floods and debris flows, as the ultimate aim of our work was to use the improved DEMs in hazard modelling. One of these was in is the Caribbean Island of Dominica, which was impacted in 2017 by Hurricane Maria, and the other in the municipality of Mocoa in Colombia, which was affected by debris flows in 2017 (See Figure 2) (NASA, 2009; Stott, 2018). To evaluate the capacity of SR in improving the quality of both freely available as well as commercial global DEM data, we collected SRTM DEM data from NASA, and WorldDEM data from TanDEM-X was provided by the German Aerospace Center (DLR) (DLR, 2010). In Dominica, the high-resolution LiDAR DEM required for evaluation was only available for part of the area (due to problems with persistent cloud cover during the data collection).

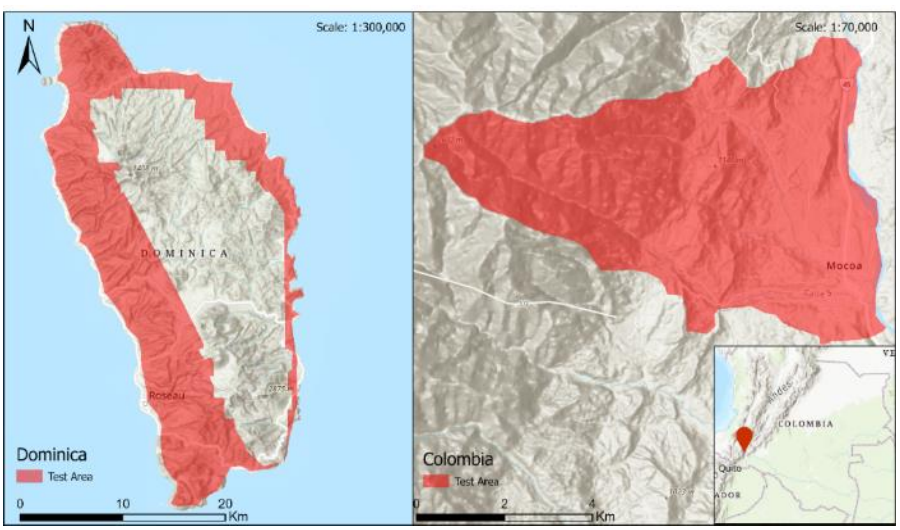

Figure 2: Inference site for global digital elevation models in Dominica and Colombia. The DEMs are clipped to match the available pixels of High-Resolution data. Basemap Sources: ESRI, HERE Corporation, OpenStreetMap.

3 Methods

The research was divided into two major phases (Figure 3); the first was developing a deep learning-based Super-Resolution model, and the second was testing the model's capacity to improve the quality of DEM data. The first stage was further divided into two tasks: model training and evaluation. For this research, we selected the best GAN-based model (ESRGAN) and Non-GAN based (EBRN) model for single image Super-Resolution tasks based on the review by Anwar et al. (2020).

The model's training was done using the freely available high-resolution DEM from Austria and its synthetic low-resolution data. After training the models, their quality and generalization were tested at the various sites in Austria using standard computer vision test approaches such as Peak Signal to Noise Ratio (PSNR), Mean Squared Error (MSE), and Structural Similarity (SSIM) (Renieblas et al., 2017). After this, the method was applied in the two test areas in Colombia and Dominica, where globally available low-resolution Digital Elevation Models were super-sampled and evaluated with locally available high resolution DEMs. To evaluate the results, mainly, two tests were developed: one statistical evaluation based on derivative maps from the DEMs and one using visual interpretation of the resulting shaded relief models by Geomorphological experts. The geomorphological tests provided qualitative information on the quality of the derived high-resolution DEM, and the analysis of the DEM derivatives was based on mathematical and statistical functions, which will be explained in the next section. The PSNR based approach could not be used in those test sites due to spatial and temporal shifts in the measurements by two different sensors.

3.1 EBRN

The Embedded Block Residual Network (EBRN) was developed by Qiu et al. (2019). It is one of the best performing models in the review by Anwar et al. (2020), with the highest value of PSNR. Unlike other models, EBRN does not process data with all frequency levels (such as elevation difference or slope steepness) through the same number of layers but has different processing levels for different data frequencies (Qiu et al., 2019). In our case, the patches with very steep slopes and flat terrain are processed through a different network depth. Having such a network structure is theoretically very beneficial for DEM data because, with different elevation changes (Slope), different processing levels are required to generate better representation. A smooth reconstruction might be useful if the terrain has low slope steepness, but more processing and reconstruction are crucial to generate better SR images for steep slopes. Furthermore, EBRN has a novel approach for block residual and its embedding through concatenation rather than stacking, proving to be better at reconstruction than the existing methods (Qiu et al., 2019).

The model is modified to take as input a single normalised elevation layer. The overall architecture of the model after modification is shown in Figure 4. The input LR image is passed through different levels of Block Residual Modules (BRM) based on their frequency (in our case, slope steepness). Each BRM aims to reconstruct the parts of higher resolution images in a specific frequency domain and pass the remaining signals to the next module, which again reconstructs some higher frequency domain (Qiu et al., 2019). The results of each nested BRM module are passed through convolution layers and subtracted from the lower-level BRM module. The results of all nested BRM modules are finally concatenated, after which the high-resolution DEM is reconstructed through several convolutional layers. Each BRM module processes the information from an input upto its capacity and then passes it to the next BRM for further processing to generate better elevation data. However, when a higher amount of processing is not required, the more complex process can produce unwanted artefacts. To reduce such problems, all the outputs are first concatenated and passed through the convolution layer. The higher number of convolution layers is better suited for the high frequency data but once all of the information is concatenated, final convolution layers will further process the data for better reconstruction.

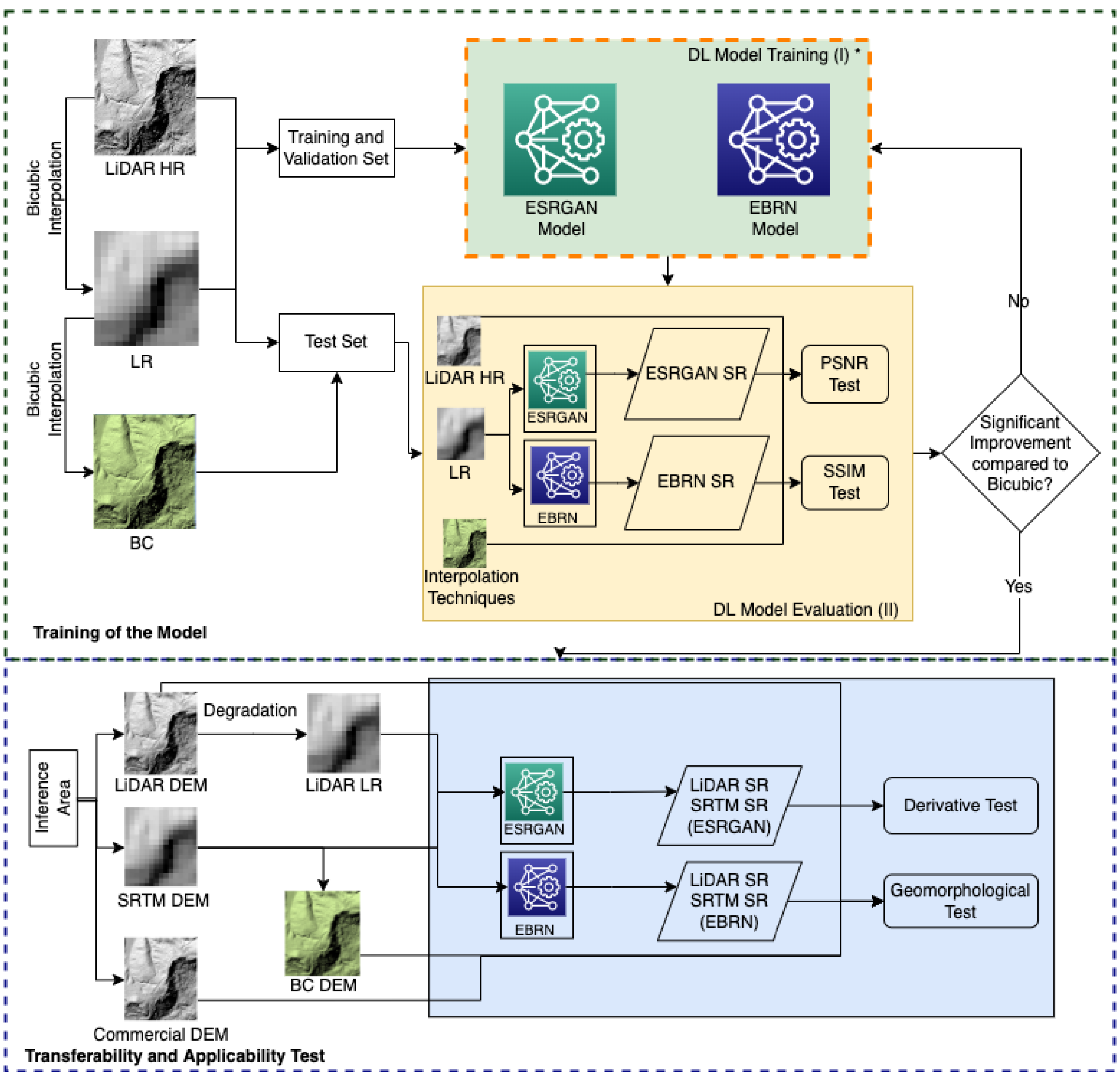

Figure 3: Research Methodology. The figure shows two different phases of research and how each phase was conducted; see the specific section for further details.

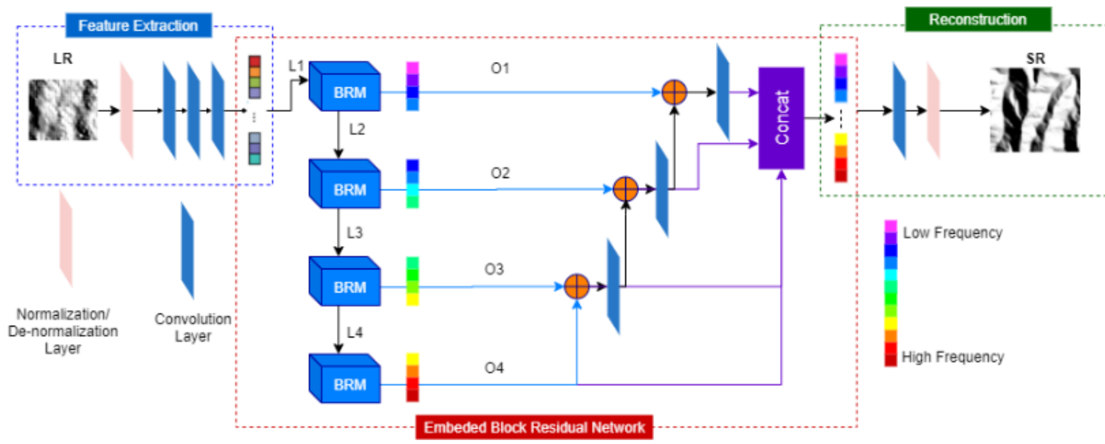

Figure 4: Embedded Block Residual Network for the Digital Elevation Model. Where O1-4 are output from each BRM module.

Qiu et al. (2019) used L1 Loss (Mean Absolute Error) (Eq 1) as the target function and then fine-tuned it using the L2 (Mean Squared Error) (Eq 2.). However, we also wanted to have the topographic features such as Slope and Aspect in the output data as close to reality possible because, when this elevation data is used in geospatial analysis, the relative elevation difference between neighbouring pixels is often more important than the absolute elevation. To minimise the relative error between the neighbouring pixels, we introduced a novel loss function called the *TopoLoss* function, as shown by equation (3). The *TopoLoss* function calculates the error between topographic properties (Slope and Aspect) obtained from the high-resolution data and the output from the SR method; in this case, we have used Slope and Aspect loss which are combined using the weighted summation. The weights were obtained by fine-tuning, and for this case, 0.7 and 0.3 were used for Slope and Aspect, respectively. The *TopoLoss* was added as a regularisation parameter to L1 Loss with weight scalars, which helps define each parameter's importance in overall model optimisation.

$$l1 = \mathbb{E}_n \left| |y - \bar{y}| \right| \qquad (1)$$

$$l2 = \mathbb{E}_{xi} \left| (y - \bar{y})^2 \right| \qquad (2)$$

$$TopoLoss = \alpha \cdot Slope\ Loss + \beta \cdot Aspect\ Loss \qquad (3)$$

Where: L1 and L2 are loss functions, y is high-resolution DEM, $\bar{y}$ is output from the SR model, and $\mathbb{E}$ is the mean value; α and β are the regularization parameters.

$$Final\ EBRN\ Loss = \gamma \cdot L1\ Loss + \delta\ TopoLoss \qquad (4)$$

Where γ, δ are weight scalars.

3.2 ESRGAN

The ESRGAN model is one of the most used models in GAN-based Super-Resolution approaches (Anwar et al., 2020). The model has two parts: a generator and a discriminator. The generator model creates the

Super-Resolution image from the low-resolution image. The discriminator model evaluates if the generated image resembles the high-resolution image; based on that, adversarial feedback is provided to the generator network as a loss function (Wang et al., 2018). The generator model of ESRGAN is composed of residual in residual blocks (see Wang et al., (2018) for further information) without any batch normalisation layers, which makes it easy to converge.

The existing ESRGAN model was modified to add the data normalisation at the start, the denormalization layer at the end of the model and the number of blocks was fixed to 20, as suggested by Wang et al. (2018). The normalization and denormalization were done in the range from 0-8000 (elevation values) to 0-1 and vice versa. The modified network architecture of the Generator model is shown in

Figure 5. When an input map is normalised and enters the basic block (residual in residual blocks which are connected sequentially), it passes through convolution and the *LeakyReLu* activation function and is combined with the *skip* connections. After it reaches the bottleneck, it is upsampled followed by two convolutions and denormalization layer producing the SR output. The last layer of the model uses the *ReLU* activation function to provide positive elevation values. Furthermore, the discriminator model of the ESRGAN model was used as suggested by Wang et al. (2018).

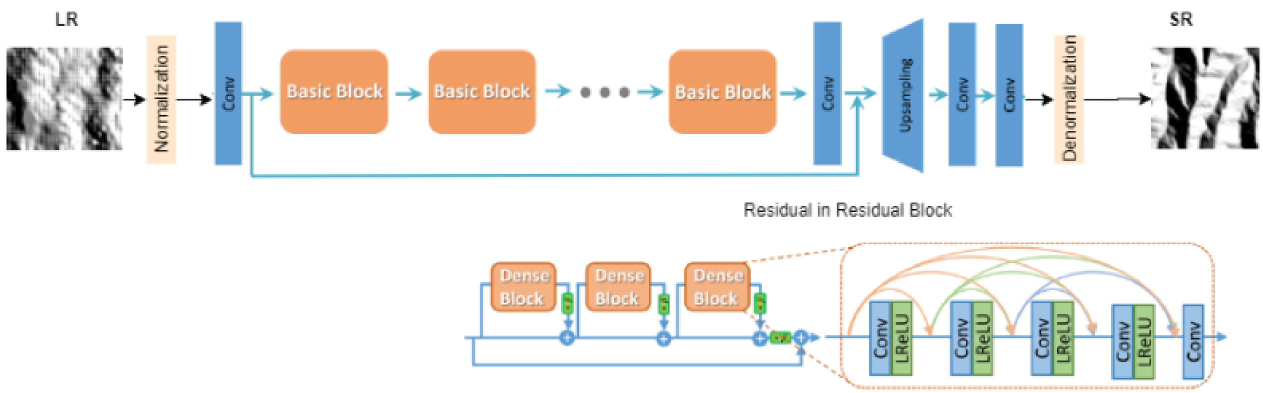

Figure 5: ESRGAN Generator model architecture. The lower image represents the Basic Block which shows the architecture of convolution layers and skip connections. Modified from Wang et al. (2018).

To improve the quality of the model and to minimise the relative elevation values, we also used the *TopoLoss* and the *L2 Loss*. For the generator and discriminator, the *Relativistic Loss* as defined by Wang et al. (2018) was used, which provides the likelihood of the SR image looking like a HR image. Since the Generator and Discriminator compete against each other in a zero-sum game, the *Relativistic Loss* for the generator is shown in Equation 5. The component of $1\text{-}D_{ra}$ (x_r, x_f) indicates how the HR data is not more realistic than SR data, and $D_{Ra}(x_f, x_r)$ how SR is less realistic than HR data. After combining the content loss and *TopoLoss* with the generator model, the final generator loss is represented by Equation (9). We did not include the *Perceptual Loss* suggested by Wang et al (2018) because, in our case, there are no distinguishable features that could be used for perception and using *Perceptual Loss* only increased the complexity of the model without much improvement.

$$\text{Disc. Relativistic Loss} = -\mathbb{E}_{xr}\left[\log\left(D_{ra}(x_r, x_f)\right)\right] - \mathbb{E}_{xf}\left[\log\left(1 - D_{ra}(x_f, x_r)\right)\right] \tag{5}$$

$$\text{Gen. Relativistic Loss} = -\mathbb{E}_{xr}\left[\log\left(1 - D_{ra}(x_r, x_f)\right)\right] - \mathbb{E}_{xf}\left[\log\left(D_{ra}(x_f, x_r)\right)\right] \tag{6}$$

$$D_{ra}(x_r, x_f) = \sigma\left(C(x_r) - \mathbb{E}\left[C(x_f)\right]\right) \tag{7}$$

$$D_{ra}(x_f, x_r) = \sigma\left(C(x_f) - \mathbb{E}\left[C(x_r)\right]\right) \tag{8}$$

$$GenLoss = \alpha L_g^{Ra} + \eta L1 + \beta\, TopoLoss \tag{9}$$

The Generator Loss function is used where *TopoLoss* is represented by topographic loss and function GenLoss is loss for the generator model. α, β, η are the scalar weights.

3.3 Super-Resolution Evaluation Methods

We selected four approaches to evaluate the super-resolution results. The first two (PSNR and SSIM) were applied to the dataset from Austria, Dominica, and Colombia, where we used high-resolution and low-resolution data from the same DEM source. The other two approaches (Derivatives and Geomorphological testing) were used in all sites where we did not have a high-resolution counterpart from the same source for low-resolution data such as SRTM. Even though LiDAR HR images were available in Dominica and Austria, it was not possible to compare them using the PSNR and SSIM approaches because the elevation values per pixel were different from both sources due to the measurement bias and noise, grid structure, quality of measurement, and acquisition dates. Therefore, we used other comparison methods: Derivative Evaluation and Geomorphological Evaluation, to suit our application.

The *Peak Signal to Noise Ratio* (PSNR) emerged from electrical engineering to measure the ratio between a signal's maximum power and the power of the noise (MATLAB, 2020). In computer vision and machine learning, it has been used frequently for quality checking of the output from different classification algorithms, and it is also a common method to check the quality of the Super-Resolution algorithms (Ledig et al., 2017). We also evaluated *Mean Squared Error* (MSE) to compare the error reduction in each method and relative comparison between improvement by both EBRN and ESRGAN. The equation for measuring PSNR is shown in Equation 10.

$$PSNR = 10 log_{10}\left(\frac{R^2}{MSE}\right) \tag{10}$$

Where R is the maximum fluctuation in the image data and depends on the image's bit depth, such as an 8-bit image will have a 256 value of R, and MSE is the Mean Square Error of the difference between generated and real image (MATLAB, 2020).

The PSNR measures the quality of the measurement based on the mean square error and does not consider the human perception and spatial variability of the images (Z. Wang & Bovik, 2009). We used the *Structural Similarity Index Measure* (SSIM) method to measure the perceived quality, which compares the image quality of the generated high-resolution image with the measured high-resolution image. The SSIM method considers the luminance (brightness), contrast, and structural information while comparing the data (Leong & Horgan, 2020). In our case, the luminance and contrast are represented by the actual ground measurement instead of the digital number, so the SSIM is expected to show very high similarity (almost 1 for all cases) compared to the natural image Super-Resolution. To better evaluate the similarity between the generated and original DEM, we used SSIM with shaded relief, which represented the grayscale image of the terrain and could represent the similarity without much bias.

When using freely available global datasets, we cannot measure the improvement using PSNR and SSIM methods because they always need a high-resolution dataset with exactly aligned pixels. In our case, the SRTM DEM and HR DEM are available to compare, but their pixels are not exactly aligned. It is more important for further geospatial analysis to have reliable derivative maps, such as slope steepness, than absolute values. To overcome that problem, we used the DEM derivative analysis method to evaluate the extent to which the bicubic and SR methods can reconstruct the topographic properties compared to high-resolution data using the Kernel Density Estimation Function. We calculated the DEM derivatives (namely Slope Steepness, Aspect, and Topographic Wetness Index) and plotted the Kernel Density estimate for each derivative. The Kernel Dnsity Estimate (KDE) function was calculated using the Seaborn library in Python. The Kernel Density Estimation function estimates the Slope, Aspect, and TWI probability density in different elevation datasets using equation 12 (Rosenblatt, 1956).

$$f = \frac{1}{nh} \sum_{i=1}^{n} K\left(\frac{x - x_i}{h}\right) \qquad (11)$$

Where: K is the Kernel, a non-negative function, h is the smoothing parameter, x is the data point, and n is the total number of data points.

To understand how SR-based approaches can perform compared to commercial data such as TanDEM-X, we performed the derivative analysis. We also performed an extensive visual and geomorphological evaluation with the help of experts to better understand how the improvement is obtained in the SR-based methods. We asked two geomorphological experts to score the quality of each output in recognizing landforms based on shaded relief images with a value between 0 and 10.

3.4 Experimentation Details

The EBRN model was trained with 80% of the training dataset, and 20% was used for validation. It was trained for 1000 epochs with checkpoints to avoid overfitting. The model was trained with Adam Optimizer

(Kingma & Ba, 2015), and the learning rate was set to 1e-04 in the beginning and then reduced by a factor of 0.5 in every 100 epochs until it reached 1e-06. The batch size for the model was 10, and there were 500 steps in each epoch. Due to the very complex combined loss functions, the model had problems converging initially, and to avoid that, we used a similar concept as curriculum learning (Bengio et al., 2009) but with increasingly complex loss functions instead of increasingly complex datasets. Initially, we used simple Mean Absolute Error, and after the model converged, we used Mean Squared Error for a better generalisation, and finally, we used a combination of L1 Loss and *TopoLoss* as suggested by Equation 7. The reason behind this was that the training process performed slow and inefficiently when we used the combined loss function without gradual complexity. To our knowledge, this is the first research to use loss functions in such a way for optimisation.

For the ESRGAN Model, the Generator model was trained first without a discriminator to avoid collapse mode because of a weak generator, followed by GAN training as suggested by Wang et al. (2018). The training was done using the Adam optimiser (Kingma & Ba, 2015) with a learning rate initially at 1e-03 and then decayed by a factor two until it reached 1e-06 for the generator. The Generator training was done in similar ways as the EBRN model with a curriculum-like training, where instead of gradually increasing the data complexity, we increased the complexity in the loss function. Firstly, the model was trained with an L1 loss followed by an L2 Loss and finally, the combination of TopoLoss and L1 Loss. Once the generator was trained for 1000 epochs, with L1 and TopoLoss, we started the GAN learning process where both generator and discriminator performed against each other for another 1000 epochs. During the GAN training, the discriminator learning rate was set to 1e-03 for faster learning in the beginning as compensation for that of the pretrained generator, and the generator learning rate was set to 1e-05. After both models converged and had reliable and satisfactory results, we stopped the training process and did model averaging. The model averaging identifies the best suitable network weights with lower artefacts, higher PSNR, and higher visual quality. This approach was suggested by Wang et al. (2018). The averaging was done between the pretrained generator network and the GAN-based trained network as in Equation 12, where we could decide the factor for each model based on our requirement of higher PSNR or visual quality images.

$$Final\ Model = \mathrm{A} \cdot G_{Pretrained} + (1 - A)G_{GAN-trained} \qquad (12)$$

This model Averaging function uses a weight A between 0-1.

After the model training, during the inference process, we had to create smaller patches according to the model shape and again combine them after prediction. We observed that the model produces noisy data in the boundaries of patches introducing artefacts in the inference boundaries. To solve that, we applied a basic photogrammetric overlap approach and developed an inferencing program so that the output parts from the SR model during inference are overlapped, as shown in Figure 6, to remove noise in bordering pixels. A similar approach has been used by Kubade et al. (2021) during the training and evaluation process, but such application would mean over-amplifying accuracy/PSNR and only falsely representing that the model has better capacity when this is not actually the case. To avoid making such mistakes to get a false impression of the model capacity, we implement this approach in inference only, so the quality of the model during training and evaluation remained

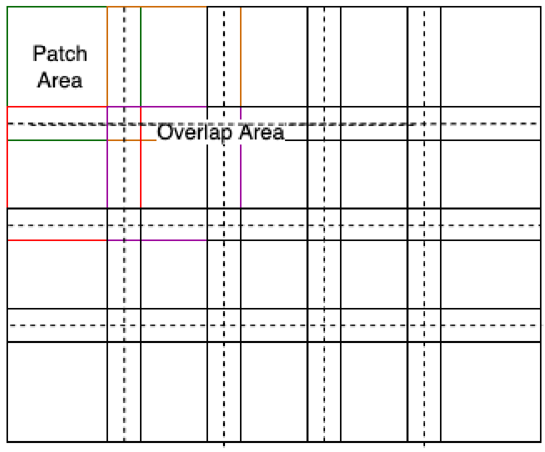

Figure 6: Overlapping of the Inference Patches. Here, the dotted lines separate the pixels used from each patch, and the bold line shows the boundary of the patches. All patches overlap, and only certain portions of the overlapping area are used.

4 Results and Analysis

The results from the SR models are shown and analyzed in this section. First, we tested the transferability of the model trained in Austria to Dominica and Colombia and then analyzed its capacity to improve the SRTM DEM in the remaining two sections. Figure 7 (left) shows the capacity of the trained model to improve the quality of LiDAR DEM using both EBRN and ESRGAN models in Dominica. As we can observe, both EBRN and ESRGAN models have increased the visual quality of the DEM while improving the degraded low-resolution LiDAR DEM to a high-resolution counterparts significantly over the bicubic method. The ESRGAN and EBRN model have very similar results even though in terms of parameters, EBRN is deep and complex, while in terms of training complexity, ESRGAN is more complex. Furthermore, the predictions made in SRTM DEM at Dominica from 30 meters to 7.5 meters are also shown in Figure 7 (right), where we can observe that the ridgelines and valley lines are much improved in the SRTM DEM compared to the LR version. Furthermore, similar observations can be made in other sites, such as Austria and Colombia, where we improved the quality of the SRTM DEM from 30 to 7.5 meters, which is represented in Figure 8. Especially, the EBRN based method has better improvement compared to the ESRGAN method, and in both cases, SR Techniques have created crisp images.

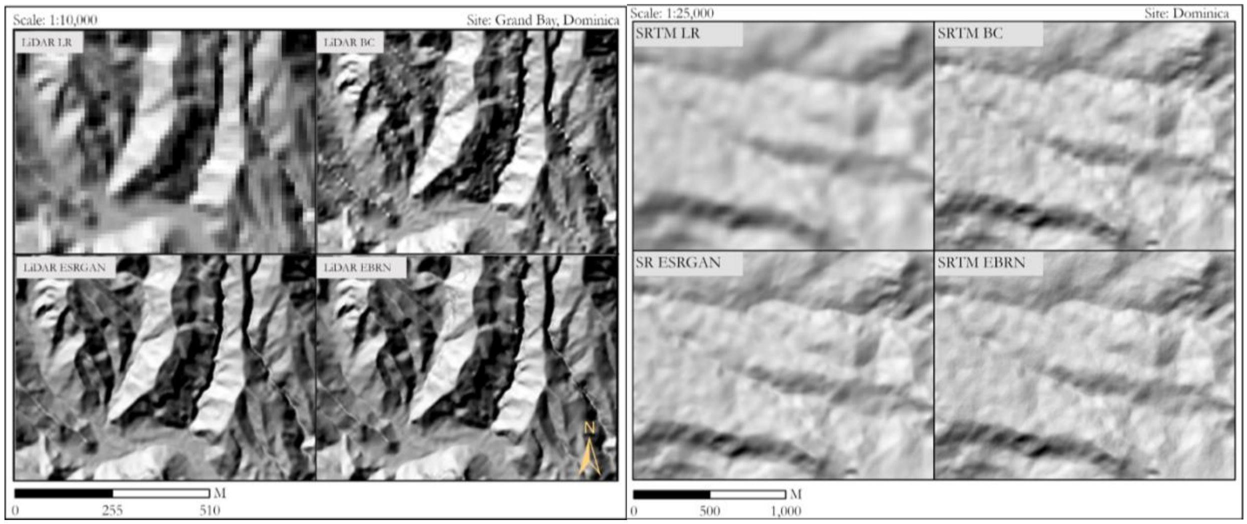

Figure 7: Example of the visual evaluation of Super-Resolution DEMs. Left: the result from the LiDAR DEM, right : the result from the SRTM DEM in different locations to show how super resolution can improve low resolution data even without much topography.

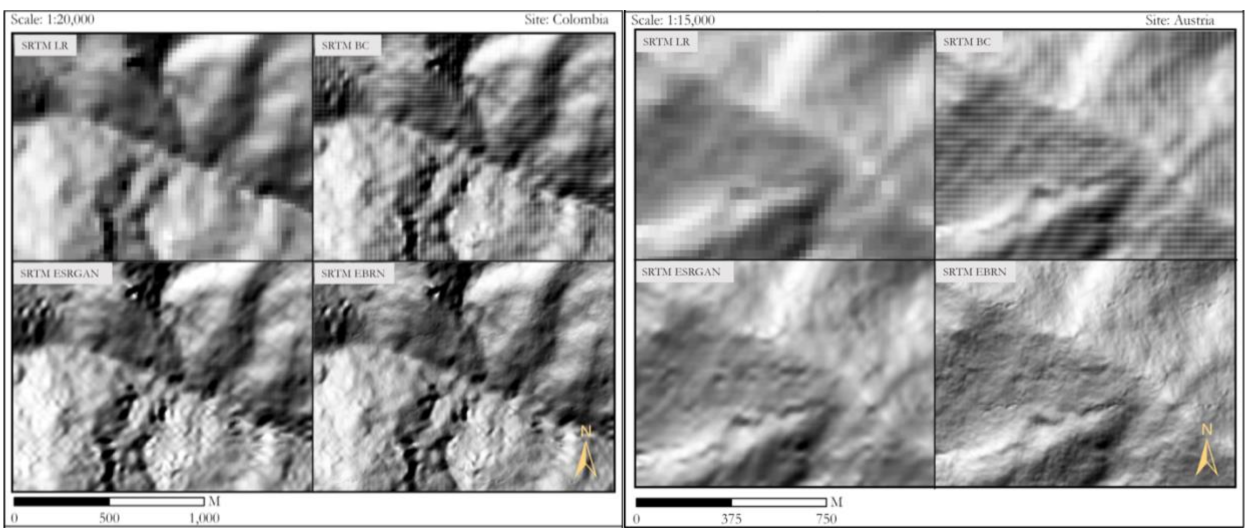

Figure 8: SRTM DEM Improvement using SR techniques in Colombia (left) and Austria (right)

4.1.1 PSNR and MSE Analysis

The PSNR results obtained for the test area in Austria and the inference area in Colombia and Dominica based on High-Resolution DEMs (mostly LiDAR) are shown in Figure 9. Both EBRN and ESRGAN based methods have improved the PSNR values compared to Bicubic Interpolation in all the study sites. As we can observe in Figure 9 (left), the Super-Resolution with DL techniques yields superior results compared to other methods in all study sites. As PSNR has a logarithmic scale, the amount of improvement is difficult to perceive; so, the model's capacity to reduce MSE error is presented in Figure 9 (right). The MSE is decreased by a significant amount in both EBRN and ESRGAN in all study areas with Super-Resolution techniques. Furthermore, we can observe that the reduction of MSE from NN (Nearest Neighbour) to BL

(Bilinear) is very high and from BL to BC is lower, and BC to SR methods are lowest; this is because once the accuracy is high, it is more difficult to improve the quality of data. All curves show the same pattern in the reduction of MSE, indicating that the model can perform similarly with different amounts of noise present in the LR data.

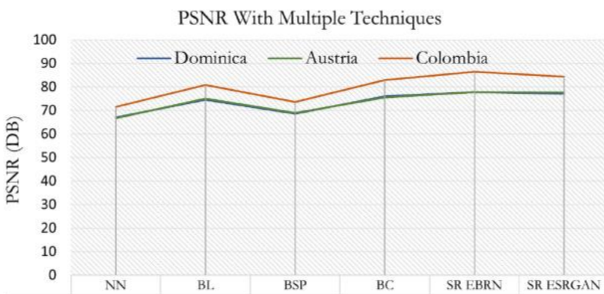

	NN	BL	BSP	BC	SR EBRN	SR ESRGAN
Dominica	67.027	74.506	68.617	75.943	77.789	77.084
Austria	66.752	75.051	68.848	75.500	77.734	77.531
Colombia	71.428	80.802	73.661	82.889	86.443	84.336

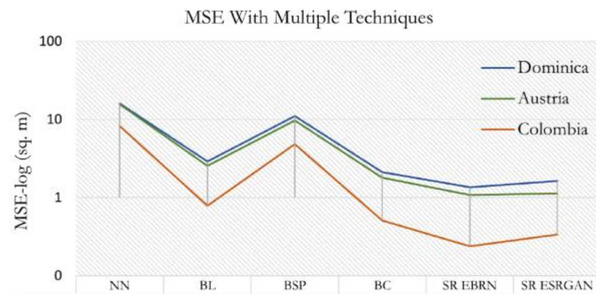

	NN	BL	BSP	BC	SR EBRN	SR ESRGAN
Dominica	15.993	2.891	11.069	2.112	1.360	1.638
Austria	15.750	2.556	9.684	1.8036933	1.0784966	1.130
Colombia	8.227	0.787	4.859	0.510	0.238	0.336

Figure 9: PSNR with different interpolation and Super-Resolution techniques (left). Mean Square Error in the different study areas with different interpolation and SR techniques. Y-axis in log scale for better representation (right).

4.1.2 SSIM

The results of the SSIM analysis using Hillshade images are shown in Figure 10, where we can observe that the SR-based approaches, specifically EBRN, have significantly improved the similarity of the the SR images to that of the HR images. Furthermore, more interesting is to see that, in the case of Hillshade images, Bilinear and Bicubic Spline interpolation methods result in better visualization than bicubic interpolation, whereas for more accurate values, Bicubic Interpolation techniques show better results. The EBRN model has shown similar characteristics in all study areas, but ESRGAN has performed better than EBRN in Austria, where it was trained but performed worse in other study areas. This behaviour is due to the architecture of the model and its quality, and as will be further discussed later. Since the SSIM evaluation is a new approach, we cannot compare our model with earlier research results in terms of visual quality improvement.

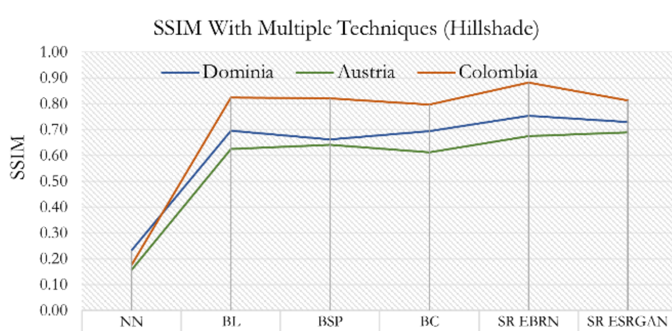

	NN	BL	BSP	BC	SR EBRN	SR ESRGAN
Dominia	0.23250	0.69599	0.66187	0.69365	0.75274	0.72911
Austria	0.15710	0.62513	0.64078	0.61172	0.67433	0.68893
Colombia	0.17689	0.82406	0.82036	0.79619	0.88110	0.81250

Figure 10: SSIM results using Hillshade Images obtained from different techniques.

4.1.3 Derivative Analysis

To understand how the global freely available, and commercial, DEM data was improved in terms of the DEM derivatives, we estimated the Kernel Density Estimation (KDE) function for all the available datasets and plotted it against high-resolution DEMs in all three study areas (Figure 11). As we can observe in Figure 11 (subplot [1,1]), for the Slope steepness in Dominica, the bicubic interpolation (red line) has its peak a bit below the peak of the EBRN, and ESRGAN methods. Both of the SR methods are performing very similar, and we can also observe that the TanDEM-X results have the slope distribution closer to that of the high-resolution DEM. Furthermore, we can observe in all three study sites that the distribution of ESRGAN and EBRN is more like the HR DEM than that of the Bicubic Interpolation method. If we observe the case of Austria, the Bicubic Interpolation has a higher number of pixels in 1.0 to 1.2 radians, but a lower number of pixels is present in the 1.2-1.5 radians range. In contrast, HR DEM has a higher number of pixels in those regions, showing that Bicubic Interpolation has smooth results, and ESRGAN and EBRN have tried to improve that to generate more pixels with the higher Slope shown by the upper peak.

In the case of Aspect, we can observe that all the resulting values are similar, except the TanDEM-X, which may be due to the higher quality of this data. What makes it more interesting is that the Aspect is not so influenced by the choice of the interpolation techniques, and is mostly comparable to the high-resolution DEM, especially in Austria and Colombia. . As we can observe in Figure 11 ([2,2] subplot), the SR-based techniques have slightly lower curves near the peak, making it more similar to the high-resolution data, but that improvement is not that significant.

For the Terrain Wetness Index (TWI), we can see that in Figure 11 (sub-image [3,3]), the TWI from EBRN is almost perfectly aligned with the HR data. The improvement, in this case, is very significant. However, in the case of Dominica, the TWI values are more clustered for each dataset, and in Colombia, even though all the values are clustered , we can observe that the ESRGAN and EBRN models are nearer to the HR data than that of the BC data. The case in Dominica is more interesting because the HR-DEM available in Dominica does not cover the major mountainous part and is covers the relatively flatter coastal areas, which might have caused such peak and clustering.

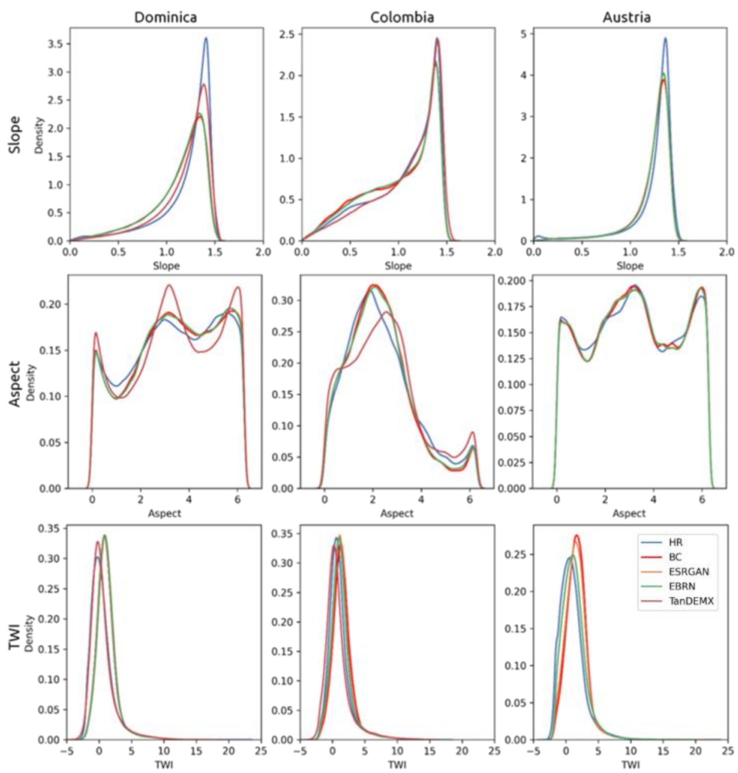

Figure 11: KDE estimation of multiple DEM and their derivatives

4.1.4 Geomorphological Analysis

The geomorphological experts evaluated the quality of the DEMs produced with the commercial DEMs by visual observation soring method, giving score between 0 (very poor) and 10 (very good). Where, experts visualized the DEM with geomorphological features identification goal and scored how easy it was to identify specific features. As we can observe from Table 1, the SRTM low-resolution DEM has the lowest score, followed by the bicubic interpolation and EBRN. The evaluation was targeted to the detection of landslides and denudational landforms, so, obviously, the HR high-resolution DEM has the highest score. The data from TanDEM-X have higher information content, and the recognizable features using this data source were also higher (Beaudry & Renner, 2012).

For the visual interpretation, on average, the ESRGAN method has a better performance in Dominica, whereas the EBRN method performed better in both other regions. However, there was disagreement among the Geomorphologist on this, as one scored EBRN as the top performer in all three sites, and the other scored ESRGAN highest, which indicates that the evaluation is subjective. In general, the ESRGAN has a better performance as the GAN-based approach is better known for its visually pleasing images (X. Wang et al., 2018).

	DEM Generation Methods

		LR SRTM	BC SRTM	EBRN SRTM	ESRGAN SRTM	TanDEM-X	HR DEM
Test Site	Dominica	0.75	2.5	3.5	4	4	8.5
	Colombia	0.75	2.5	3.5	3.5	5	8.25
	Austria	0.75	3	4	3.75	NA	9.5
Average Score		0.750	2.667	3.667	3.750	4.500	8.750

Table 1: Geomorphological score of different methods for DEM resolution improvement.

The geomorphologists concluded that LiDAR has the best performance, even though many landscape features were not very clearly visible. Furthermore, they also commented that the TanDEM-X has a highly mottled/speckled structure. The SRTM low-resolution data was very coarse and had rounded terrain forms, and both EBRN and ESRGAN had smoother surfaces than bicubic, but landslide detection was still not possible.. In the case of Austria, the LiDAR DEM had a very good image quality where all geomorphological features were clearly visible, but in the case of other DEMs, it was very difficult to recognize those features and interpret them.

In summary, the geomorphologists suggested that the SR images were not better in terms of recognizing the geomorphological features, as also a pixel size of 7.5 meters is too large for any good quality recognition of geomorphological features.

5 Discussion

Earlier research on Super Resolution of images has used different algorithms and data from different locations and with different peak values for PSNR, which make it difficult to compare our results with earlier work (Argudo et al., 2018; Chen et al., 2016; Demiray et al., 2020; Jiao et al., 2020; Kubade et al., 2020, 2021; Shin & Spittle, 2019b; Wu & Ma, 2020). Furthermore, unlike computer vision Super-Resolution, where existing test datasets are available for a fair comparison between algorithms, in the geoscience community, especially for DEM data, there is no standard dataset for comparison of the improvement, making it impossible to compare the performance of our approach relative to others. Even though the works of Argudo, Chica, & Andujar (2018) (FCND Model) and Kubade et al. (2020, 2021) (DSRFB-2020 and AFND-2021) have used data from Austria, resolution of the data they used is 2 meters compared to our five meters (in LIDAR DEM) making it incomparable. Results by Kubade et al. (2020, 2021), which include RGB images and overlapping in the model, are also not comparable because we do not have included any auxiliary information and overlapping can cause false overrepresentation of accuracy by removing problematic pixels in patch edges. For our purpose, we cannot include high resolution satellite imagery in very high-resolution range because we tried to create method that can be used in various geoscientific data where such auxiliary information might not be available as well as acquiring very high-resolution images could also be expensive in many cases.

One possible way to perform an evaluation of the model results is to compare the model's capacity to reduce the squared root of standard deviation in error (MSE), which shows the capacity of the model to reduce the noise and random error compared to a basic bicubic interpolation. This approach is less biased to the dataset location than the reduction of mean error, but not completely without any bias and should be considered as relative information. The comparison of our results with the work of others is shown in Table 2. The standard deviation in RMSE has been significantly decreased by both models compared to earlier reported values (Xu et al., 2019; , Sun et al., 2011;, Chen et al., 2016;,

Model Name	Reference	AVG RMSE	SRSD	Avg St. Dev Improvement in RMSE
Xu et al., 2019	Xu et al., 2019	13.635	1.952	
BP	Xu et al., 2019	11.136	1.882	3.586%
Sun11	Sun et al., 2011	10.782	1.885	3.432%
D-SRCNN	Chen et al., 2016	10.962	1.919	1.691%
DGPN(SRCNN)	Xu et al., 2019	10.130	1.798	7.889%
DGPN(EDSR)	Xu et al., 2019	9.785	1.805	7.531%
Bicubic	This study	1.170	2.127	
EBRN		0.898	1.681	20.957%
ESRGAN		0.974	1.813	14.780%

Table 2: Comparison of standard deviation reduction by different methods for the different datasets. AVG RMSE: average Root Mean Square Error; SRSD: Square Root of Standard Deviation in MSE

While comparing the quality of our model to that of other published work, we realized that it is crucial to have a standard dataset for modelling and comparing the quality of the model for geoscience data. In the case of computer vision, there are many such reference data available such as DIV2K (Agustsson & Timofte, 2017), General100(Dong et al., 2016), and MANGA109 (Aizawa et al., 2020), which are used in training and testing the model. However, as we mentioned earlier, due to the lack of such a dataset in the geoscience community, it is very difficult to compare the quality of the model and its output.

Wu & Ma (2020) used the SSIM Index, but the change in SSIM with DEM SR was on the scale of 1e-5, which makes it very difficult to understand if there is an improvement. Our approach of using SSIM with DEM derivatives has proven to be a better metric to measure the improvement in the visual quality of the image. The quantitative comparison using methods such as RMSE, MSE and other methods described by Polidori & Hage (2020) was not possible due to the lack of ground truth data. We could have used the HR DEM as ground truth but at the same pixel location of HR DEM and SRTM DEM the elevation values were slightly different because of their resolution at the time of data collection. SRTM being collected at much lower resolution had error in the vertical direction whereas LIDAR DEM has much less error. Due to such error direct comparison of model's performance using these two datasets is not possible. Figure 12 shows cross sections from SRTM and LIDAR HR in Dominica illustrating that both DEMs have some similar data in some places and completely different values in others. To overcome this problem, we used the derivative, visual and geomorphological analysis.

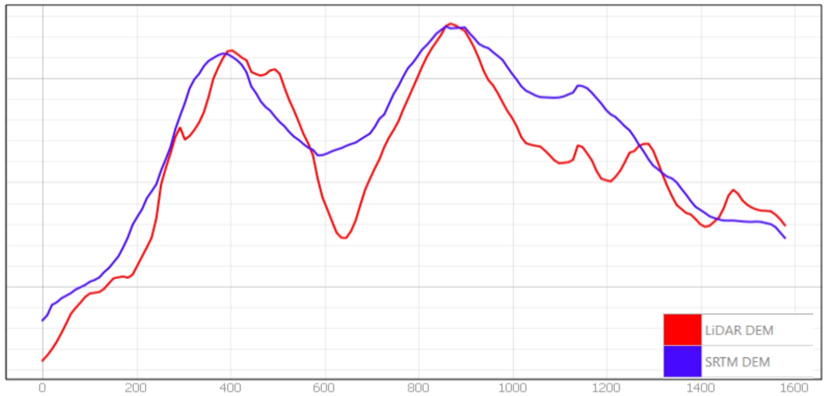

Figure 12: Cross section of a test area in Dominica demonstrating the randomness in difference in elevation values between SRTM and LiDAR DEMs. The X-Axis represents distance, and Y-Axis represents elevation.

The results of the visual comparison are self-explanatory, but a few things are worth discussing. Both of the SR model better preserved the ridges and the valley lines as compared to bicubic interpolation, but the various SR DEMs show also large differences related to data processing inequality (Beaudry & Renner, 2012). In most of the terrain, detailed features on mountain slopes are not visible in the SRTM DEM, making it impossible to generate them via SR methods. Without any indication of these features in LR data, the SR models start to create artefacts, and increase the noise in the model. However, in those cases where ridge and valley lines are visible in the SRTM DEM, the SR-based methods have created a very good representation. This limits the use of SR-based methods in mapping the geomorphological features, which are not available in the LR dataset.

Another important point in the visual analysis is that the ESRGAN based method results generally in smoother terrain than the EBRN results, due to the different model architecture. The EBRN model processes a different frequency of information with a different level and complexity, whereas ESRGAN passes all of them through the same network. When the model was trained, we used a high-resolution DEM and its degraded counterpart, which was better in visual quality than the SRTM LR used in Dominica and Colombia. We did not used the combination of LiDAR and SRTM DEM as training pairs because of their pixel-by-pixel noise distribution and which occurs randomly and this reduces the generalization capacity of the model making it unusable in other locations. The ESRGAN Generator model learned to generate HR data from those perfectly created bicubic samples, but it had more difficulty in providing good quality data from SRTM DEMs.. On the other hand, the EBRN model has different processing complexity, and when it was trained, all the blocks had their weights, and when we provided more noisy data, it could pass it through more complex blocks to generate a dataset with higher visual quality.

In the end, it is very difficult to decide which model works better in the case of SR, but a reasonable choice can be made by comparing the number of parameters to be trained. To further evaluate our work, we plotted the percentage improvement in MSE versus the number of model parameters in Figure 13. The model improvement in the EBRN model is greater in terms of MSE improvement than in the ESRGAN model, which is similar to the observation of Anwar et al. (2020). EBRN is a PSNR oriented model and processes the different data frequencies with different model depths; the model's performance is better in the inference area. The number of parameters for the EBRN model is higher (3x) than the ESRGAN Generator model, but being a Non-Generative model, it is easier to train the EBRN model even though the training process is slower compared to training the ESRGAN model (Kodali et al., 2017). Since the ESRGAN model is more focused on visually better images, the ESRGAN output for Austria has higher SSIM, as shown in the results section, but EBRN has shown better performance in terms of inference. In terms of improving the quality of DEM, the EBRN model is better.

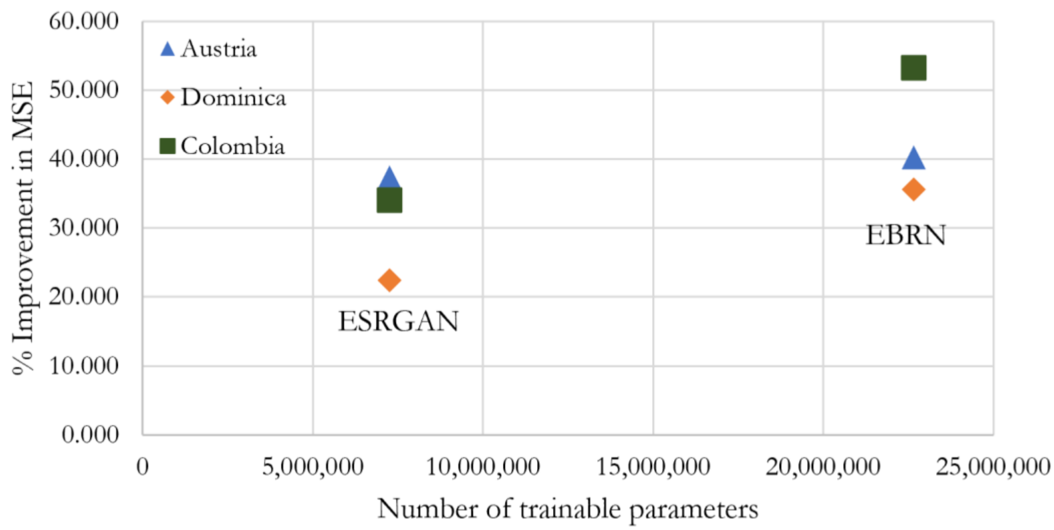

Figure 13: Improvement in MSE by model vs the complexity of the model

6 Conclusion and Future Directions

Our research shows that SR based methods can be used to improve the globally available free and open Digital Elevation Models. The SR-based models also have shown an excellent capacity to increase the spatial variability and crispness in the images compared to traditional techniques such as bicubic interpolation. Furthermore, in the case of application on a global dataset with many uncertainties, the ESRGAN based model is more suitable than the EBRN model because of its generative nature. EBRN can be more useful to produce more accurate results when the input low resolution data has less noise presence. In contrast, in the case of higher visual quality and derivative reconstruction, the ESRGAN based model is suited to increase the crispness and generate better-looking images. We have also demonstrated that even though computationally complex, the ESRGAN model is more flexible to a different type of noise present in the input data due to its generative nature and can perform similarly to EBRN in data with lesser noise.

For further improvement of the work, we recommend the loss function that we developed could be further improved by including other topographic characteristics in the loss function, such as the TWI error function, error in channel location, a function to estimate the error in drainage density etc. This is likely to improve the quality of geoscientific models. The data that we used in training the current model is from Austria, which might not work well in cases of very different terrains. To improve such quality, the addition of more data from different terrain types would help generate a global model that can generate better global free data. Furthermore, there is still a need to develop public training and testing data and standard evaluation methods for geoscientific Super-Resolution, which will make it possible to compare different models and their quality without bias.

References

Agustsson, E., & Timofte, R. (2017). NTIRE 2017 Challenge on Single Image Super-Resolution: Dataset and Study. *IEEE Computer Society Conference on Computer Vision and Pattern Recognition Workshops*, *2017-July*, 1122–1131. https://doi.org/10.1109/CVPRW.2017.150

Aizawa, K., Fujimoto, A., Otsubo, A., Ogawa, T., Matsui, Y., Tsubota, K., & Ikuta, H. (2020). Building a Manga Dataset "Manga109" with Annotations for Multimedia Applications. *IEEE Multimedia*, *27*(2), 8–18. https://doi.org/10.1109/MMUL.2020.2987895

Al-falluji, R., Guirguis, S., & Youssif, A. (2017). Single Image Super-Resolution Algorithms: A Survey and Evaluation. *International Journal of Advanced Research in Computer Engineering & Technology (IJARCET)*, *6*(9), 2278–1323.

Anwar, S., Khan, S., & Barnes, N. (2020). A Deep Journey into Super-resolution: A Survey. In *ACM Computing Surveys* (Vol. 53, Issue 3). https://doi.org/10.1145/3390462

Argudo, O., Chica, A., & Andujar, C. (2018). Terrain super-resolution through aerial imagery and fully convolutional networks. *Computer Graphics Forum*, *37*(2), 101–110. https://doi.org/10.1111/cgf.13345

Beaudry, N. J., & Renner, R. (2012). An intuitive proof of the data processing inequality. *Quantum Information and Computation*, *12*(5–6), 432–441. https://doi.org/10.26421/qic12.5-6-4

Bengio, Y., Louradour, J., Collobert, R., & Weston, J. (2009). Curriculum learning. *ACM International Conference Proceeding Series*, *382*. https://doi.org/10.1145/1553374.1553380

Bhunia, G. S., Shit, P. K., & Maiti, R. (2018). Comparison of GIS-based interpolation methods for spatial distribution of soil organic carbon (SOC). *Journal of the Saudi Society of Agricultural Sciences*, *17*(2), 114–126. https://doi.org/10.1016/j.jssas.2016.02.001

Bulyshev, A., Vanek, M., Amzajerdian, F., Pierrottet, D., Hines, G., & Reisse, R. (2011). A super-resolution algorithm for enhancement of FLASH LIDAR data. *Computational Imaging IX*, *7873*, 78730F. https://doi.org/10.1117/12.876283

Chen, Z., Wang, X., Xu, Z., & Hou, W. (2016). CONVOLUTIONAL NEURAL NETWORK BASED DEM SUPER RESOLUTION. *ISPRS - International Archives of the Photogrammetry, Remote Sensing and Spatial Information Sciences*, *XLI-B3*, 247–250. https://doi.org/10.5194/isprs-archives-xli-b3-247-2016

Chu, M., Xie, Y., Mayer, J., Leal-Taixé, L., & Thuerey, N. (2020). Learning temporal coherence via self-supervision for GAN-based video generation. *ACM Transactions on Graphics*, *39*(4). https://doi.org/10.1145/3386569.3392457

Demiray, B. Z., Sit, M., & Demir, I. (2020). D-SRGAN: DEM Super-Resolution with Generative Adversarial Networks. *SN Ccomputer Science*, *2*, 48. https://doi.org/10.31223/osf.io/frd8x

DLR. (2010). *TanDEM-X - the Earth in three dimensions* . German Aerospace Center. https://www.dlr.de/content/en/missions/tandem-x.html

Dong, C., Loy, C. C., & Tang, X. (2016). Accelerating the Super-Resolution Convolutional Neural Network. *Lecture Notes in Computer Science (Including Subseries Lecture Notes in Artificial Intelligence and Lecture Notes in Bioinformatics), 9906 LNCS*, 391–407.

Ji, X., Cao, Y., Tai, Y., Wang, C., Li, J., & Huang, F. (2020). Real-world super-resolution via kernel estimation and noise injection. *IEEE Computer Society Conference on Computer Vision and Pattern Recognition Workshops*, *2020-June*, 1914–1923. https://doi.org/10.1109/CVPRW50498.2020.00241

Jiao, D., Wang, D., Lv, H., & Peng, Y. (2020). Super-resolution reconstruction of a digital elevation model based on a deep residual network. *Open Geosciences*, *12*(1), 1369–1382. https://doi.org/10.1515/geo-2020-0207

Kingma, D. P., & Ba, J. L. (2015). Adam: A method for stochastic optimisation. *3rd International Conference on Learning Representations, ICLR 2015 - Conference Track Proceedings*.

Kodali, N., Abernethy, J., Hays, J., & Kira, Z. (2017). On Convergence and Stability of GANs. *ArXiv: Artificial Intelligence*, *1705.07215*, 1–18.

Kubade, A., Patel, D., Sharma, A., & Rajan, K. S. (2021). AFN: Attentional Feedback Network Based 3D Terrain Super-Resolution. In *Lecture Notes in Computer Science (including subseries Lecture Notes in Artificial Intelligence and Lecture Notes in Bioinformatics): Vol. 12622 LNCS*. Springer International Publishing. https://doi.org/10.1007/978-3-030-69525-5_12

Kubade, A., Sharma, A., & Rajan, K. S. (2020). Feedback Neural Network Based Super-Resolution of DEM for Generating High Fidelity Features. *International Geoscience and Remote Sensing Symposium (IGARSS)*, 1671–1674. https://doi.org/10.1109/IGARSS39084.2020.9323310

Ledig, C., Theis, L., Huszár, F., Caballero, J., Cunningham, A., Acosta, A., Aitken, A., Tejani, A., Totz, J., Wang, Z., & Shi, W. (2017). Photo-realistic single image super-resolution using a generative adversarial network. *Proceedings - 30th IEEE Conference on Computer Vision and Pattern Recognition, CVPR 2017*, *2017-Janua*(12), 105–114. https://doi.org/10.1109/CVPR.2017.19

Leong, W. J., & Horgan, H. J. (2020). DeepBedMap: Using a deep neural network to better resolve the bed topography of Antarctica. *The Cryosphere Discussions*, 1–27. https://doi.org/10.5194/tc-2020-74

Liu, C., Du, W., & Tian, X. (2018). Lunar DEM Super-resolution reconstruction via sparse representation. *Proceedings - 2017 10th International Congress on Image and Signal Processing, BioMedical Engineering and Informatics, CISP-BMEI 2017*, *2018-Janua*, 1–5. https://doi.org/10.1109/CISP-BMEI.2017.8301904

Luo, Y., Zhou, L., Wang, S., & Wang, Z. (2017). Video Satellite Imagery Super Resolution via Convolutional Neural Networks. *IEEE Geoscience and Remote Sensing Letters*, *14*(12), 2398–2402. https://doi.org/10.1109/LGRS.2017.2766204

MATLAB. (2020). *Compute peak signal-to-noise ratio (PSNR) between images - Simulink - MathWorks Benelux*. MathWorks. https://nl.mathworks.com/help/vision/ref/psnr.html

Moon, S. H., & Choi, H. L. (2016). Super-resolution based on deep learning technique for constructing digital elevation model. *AIAA Space and Astronautics Forum and Exposition, SPACE 2016*. https://doi.org/10.2514/6.2016-5608

NASA. (2009, June). *ASTER Global Digital Elevation Map*. Jet Propulsion Laboratory. https://asterweb.jpl.nasa.gov/gdem.asp

Polidori, L., & Hage, M. El. (2020). Digital elevation model quality assessment methods: A critical review. In *Remote Sensing* (Vol. 12, Issue 21, pp. 1–36). MDPI AG. https://doi.org/10.3390/rs12213522

Qiu, Y., Wang, R., Tao, D., & Cheng, J. (2019). Embedded block residual network: A recursive restoration model for single-image super-resolution. *Proceedings of the IEEE International Conference on Computer Vision*, *2019-Octob*, 4179–4188. https://doi.org/10.1109/ICCV.2019.00428

Rata, M., Douaoui, A., Larid, M., & Douaik, A. (2020). Comparison of geostatistical interpolation methods to map annual rainfall in the Chéliff watershed, Algeria. *Theoretical and Applied Climatology*, *141*(3–4), 1009–1024. https://doi.org/10.1007/s00704-020-03218-z

Renieblas, G. P., Nogués, A. T., González, A. M., Gómez-Leon, N., & del Castillo, E. G. (2017). Structural similarity index family for image quality assessment in radiological images. *Journal of Medical Imaging*, *4*(3), 035501. https://doi.org/10.1117/1.jmi.4.3.035501

Rosenblatt, M. (1956). Remarks on Some Nonparametric Estimates of a Density Function. *The Annals of Mathematical Statistics*, *27*(3), 832–837. https://doi.org/10.1214/aoms/1177728190

Shin, D., & Spittle, S. (2019a). LoGSRN: Deep super resolution network for digital elevation model. *Conference Proceedings - IEEE International Conference on Systems, Man and Cybernetics*, *2019-Octob*, 3060–3065. https://doi.org/10.1109/SMC.2019.8914037

Shin, D., & Spittle, S. (2019b). LoGSRN: Deep super resolution network for digital elevation model. *Conference Proceedings - IEEE International Conference on Systems, Man and Cybernetics*, *2019-Octob*, 3060–3065. https://doi.org/10.1109/SMC.2019.8914037

Stott, R. (2018). The World Bank. In *The World Bank*. https://doi.org/10.1136/bmj.318.7187.822

Sun, J., Xu, Z., & Shum, H. Y. (2011). Gradient profile prior and its applications in image super-resolution and enhancement. *IEEE Transactions on Image Processing*, *20*(6), 1529–1542. https://doi.org/10.1109/TIP.2010.2095871

Wang, X., Yu, K., Wu, S., Gu, J., Liu, Y., Dong, C., Qiao, Y., & Loy, C. C. (2018). ESRGAN: Enhanced super-resolution generative adversarial networks. *Lecture Notes in Computer Science (Including Subseries Lecture Notes in Artificial Intelligence and Lecture Notes in Bioinformatics)*, *11133 LNCS*, 63–79. https://doi.org/10.1007/978-3-030-11021-5_5

Wang, Z., & Bovik, A. C. (2009). Mean squared error: Lot it or leave it? A new look at signal fidelity measures. *IEEE Signal Processing Magazine*, *26*(1), 98–117. https://doi.org/10.1109/MSP.2008.930649

Wu, Z., & Ma, P. (2020). ESRGAN-based DEM super-resolution for enhanced slope deformation monitoring in lantau island of Hong Kong. *International Archives of the Photogrammetry, Remote Sensing and Spatial Information Sciences - ISPRS Archives*, *43*(B3), 351–356. https://doi.org/10.5194/isprs-archives-XLIII-B3-2020-351-2020

Xu, Z., Chen, Z., Yi, W., Gui, Q., Hou, W., & Ding, M. (2019). Deep gradient prior network for DEM super-resolution: Transfer learning from image to DEM. *ISPRS Journal of Photogrammetry and Remote Sensing*, *150*(August 2018), 80–90. https://doi.org/10.1016/j.isprsjprs.2019.02.008

Yang, J., & Huang, T. (2017). Image super-resolution: Historical overview and future challenges. In *Super-Resolution Imaging* (1st ed., pp. 1–33). CRC Press. https://doi.org/10.1201/9781439819319